A Parameterized Linear Magnetic Equivalent Circuit for Air Core Radial Flux Coaxial Magnetic Gears with Halbach Arrays

Matthew C. Gardner
Dept. of Elec. And Comp. Engr.
Texas A&M University
College Station, Texas 77843
gardner1100@tamu.edu

Derek A. Janak
Dept. of Elec. And Comp. Engr.
Texas A&M University
College Station, Texas 77843
dajanak@tamu.edu

Hamid A. Toliyat
Dept. of Elec. And Comp. Engr.
Texas A&M University
College Station, Texas 77843
toliyat@tamu.edu

***Abstract*—This paper describes a systematic way to create a 2D linear magnetic equivalent circuit (MEC) from node cells in a radial flux coaxial magnetic gear with Halbach arrays and without back irons. Three base designs are used to validate the accuracy of the MEC against a nonlinear 2D FEA in terms of torque and air gap flux densities. Guidelines based on each design's pole arcs are presented for distributing the node cells inside the inner ring of magnets and outside the outer ring of magnets. Based on these guidelines, an extensive parametric study is performed to compare the MEC and FEA results. The MEC is able to very accurately track design parameter trends. Even for the worst cases, the MEC predicts a torque within 6.9% of the FEA for a relatively coarse node cell mesh and within 4.2% with a finer mesh. However, the MEC is significantly faster than the FEA. With the coarser mesh, the MEC is almost two orders of magnitude faster than the FEA. Thus, this systematic linear MEC can be a useful tool for performing rapid initial optimizations.**

Keywords—air core, finite element analysis, Halbach arrays, magnetic equivalent circuit, magnetic gear, optimization, permeance network, radial flux, reluctance network, torque density.

I. Introduction

Like mechanical gears, magnetic gears convert energy between low-speed, high-torque rotation and high-speed, low-torque rotation. However, magnetic gears employ modulated magnetic fields, instead of mechanically intermeshing teeth. This provides several potential advantages over mechanical gears, such as improved reliability, reduced acoustic noise, reduced maintenance requirements, and inherent overload protection. Thus, magnetic gears have recently attracted significant attention [1]-[4] and have been proposed for a wide range of applications from wind [5], [6] and wave [7], [8] energy harvesting to aerospace [9], [10]. For some applications, such as those in aerospace, minimizing the mass of the magnetic gear is a critical objective. One means of reducing the mass is to mount the permanent magnets (PMs) on a relatively light, nonmagnetic material, such as plastic, instead of on magnetic steel back irons. However, using such an "air core" topology significantly increases the reluctance of the magnetic flux paths. This can be counteracted by using a Halbach array, which focuses most of the flux on a single side of the array, while reducing the flux on the opposite side of the array. Additionally, Halbach arrays have been employed in magnetic gears to reduce torque ripple, increase torque density, and improve efficiency [11]-[13]. Fig. 1(a) shows a conventional radial flux coaxial magnetic gear with surface PMs and Fig. 1(b) illustrates an air core radial flux coaxial magnetic gear with discrete Halbach arrays.

For optimal flux modulation in a coaxial magnetic gear, the number of modulators, Q_M, should be the sum of the pole pairs on the inner and outer rotors, P_{In} and P_{Out}, respectively, as given by

$$Q_M = P_{In} + P_{Out}\,. \tag{1}$$

Any one of the three bodies (the inner rotor, the outer rotor, and the modulators assembly) can be fixed while the other two are rotated with a fixed gear ratio. However, the highest gear ratio and low speed rotor stall torque are achieved if the outer rotor is held stationary. Then, the inner rotor serves as the high speed rotor, and the modulators assembly serves as the low speed rotor with the gear ratio, G, given by

$$G = \frac{\omega_{In}}{\omega_{Mods}} = \frac{Q_M}{P_{In}}, \tag{2}$$

where ω_{In} and ω_{Mods} are the speeds of the inner rotor and modulators assembly, respectively.

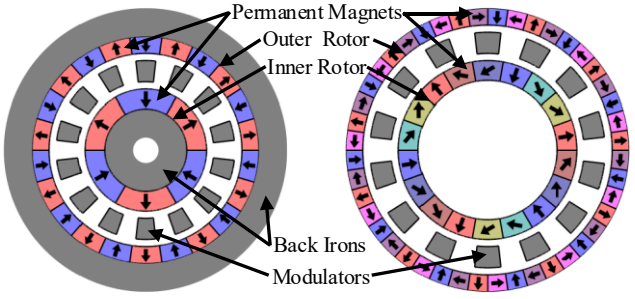

Fig. 1. Magnetically active portions of (a) convention surface PM and (b) air core Halbach array radial flux coaxial magnetic gears.

This work was supported in part by a Texas A&M Energy Institute Fellowship.

While finite element analysis (FEA) is the most common means of evaluating magnetic gears due to its accuracy and flexibility, [14] proposed a systematic means of parametrizing and forming a 2D magnetic equivalent circuit (MEC) model for magnetic gears. Unlike many traditional MEC models, which use a relatively small number of flux tubes to model the main flux paths, the proposed MEC consists of a large mesh of node cells with flux tubes connecting each node cell to the adjacent node cells. Using this model, discretization principles were developed to reduce evaluation time without biasing the results in favor of some subset of the designs [15]. This enabled the MEC model to achieve almost comparable accuracy to the FEA with significantly quicker evaluation times for a wide range of magnetic gear designs [15]. This paper adapts the MEC model proposed in [14] for air core radial flux coaxial magnetic gears with Halbach arrays. Then, it applies this adapted MEC model to three base designs and develops discretization guidelines. Finally, it presents a comparison of the torque predictions of the MEC with those of a 2D nonlinear FEA for a broad simulation study to demonstrate the MEC model's level of accuracy.

II. MEC Adaptation

The basic principle of the MEC is to create a magnetic circuit of lumped elements analogous to a lumped element electrical circuit. As in [14], the magnetic gear is divided into node cells with radial and tangential flux tubes. Then, the system can be solved for the magneto-motive force (MMF) potentials at each node in the MEC using

$$\mathcal{P}_{2D}\,\mathcal{F}_{2D} = \Phi_{2D}\,, \tag{3}$$

where $\mathcal{P}_{2D}$ is the 2D system permeance matrix, $\mathcal{F}_{2D}$ is the column vector of unknown potentials for the nodes in the 2D MEC, and Φ_{2D} is the column vector of the algebraic sums of the injected fluxes entering each node in the MEC. Once the node potentials are known, the flux densities in each flux tube can be determined, which can be used to evaluate various performance metrics, such as torque.

The first major adaptation results from removing the back irons. With adequately thick back irons, negligible flux escapes beyond the outer back iron or into the bore of the magnetic gear, as assumed in [14], [15]. However, in air core designs, flux does travel through these air regions. Thus, the two discretization parameters for the number of radial layers in the back irons are replaced with four new parameters, T_{AR1}, T_{AR2}, $N_{RL,AR1}$, and $N_{RL,AR2}$, which are the thicknesses of the inner and outer air regions included in the model and the number of radial layers in the inner and outer air regions, respectively.

The other major difference is that the Halbach arrays include PMs with some degree of tangential magnetization. As with the radially oriented flux tube in [14], a tangentially oriented flux tube containing part of a tangentially magnetized PM can be modeled using its Norton equivalent, which is the permeance of the flux tube in parallel with an injected flux, $\Phi_{inj,tan}$, which is given by

$$\Phi_{inj,tan} = (r_{Out} - r_{In})\,B_r\,\Delta z\,, \tag{4}$$

where r_{Out} and r_{In} are the outer and inner radii of the flux tube, respectively, Δz is the axial length of the flux tube, and B_r is the remanence of the PM. For PMs magnetized at an arbitrary angle, the injected flux can be divided into radial and tangential components, which are placed in parallel with the radial and tangential permeances, respectively. Additionally, when a flux tube contains portions of multiple PMs with different magnetizations, a weighted average of the magnetizations is used to determine the net injected flux.

Fig. 2(a) illustrates the flux paths in an impractically sparse MEC implementation of an example air core magnetic gear with Halbach arrays. The red lines represent the flux paths connecting each of the nodes (red dots). This sparse implementation has $N_{AL} = 24$, $N_{RL,AR1} = 3$, $N_{RL,PM1} = 2$, $N_{RL,AG1} = 1$, $N_{RL,Mods} = 3$, $N_{RL,AG2} = 1$, $N_{RL,PM2} = 2$, and $N_{RL,AR2} = 3$, where N_{AL} is the number of angular (or tangential layers) in the model and $N_{RL,PM1}$, $N_{RL,AG1}$, $N_{RL,Mods}$, $N_{RL,AG2}$, and $N_{RL,PM2}$ are the number of radial layers in the inner PMs, the inner air gap, the modulators, the outer air gap, and the outer PMs, respectively. Fig. 2(b) shows the basic 2D node cell with both tangentially and radially injected fluxes. In regions without PMs, the injected fluxes can simply be eliminated. Based on such a network of node cells, as illustrated in Fig. 2(a), the permeance matrix, $\mathcal{P}_{2D}$ can be formed based on (14)-(16) in [14]. However, based on the node cell in Fig. 2(b), the fundamental node equation ((12) in [14]) becomes

$$\sum_{i=1}^{4}\left(\mathcal{P}_i\mathcal{F}_x - \mathcal{P}_i\mathcal{F}_i\right) = -\Phi_{inj,1} - \Phi_{inj,2} + \Phi_{inj,3} + \Phi_{inj,4}\,. \tag{5}$$

Thus, the injected flux vector, Φ_{2D}, in the matrix equation (3) should be the sum of all the injected fluxes connected to the node, including both the radially and tangentially directed fluxes. Fig. 3 illustrates the MEC by overlaying the node cells of an extremely course mesh on an unrolled linear representation of a simplistic magnetic gear with $P_{In} = 1$, $P_{Out} = 2$, $Q_M = 3$, and two pieces per pole in the Halbach arrays on both the inner and outer rotors. This extremely coarse mesh has $N_{AL} = 7$, $N_{RL,AR1} = 1$, $N_{RL,PM1} = 1$, $N_{RL,AG1} = 1$, $N_{RL,Mods} = 2$, $N_{RL,AG2} = 1$, $N_{RL,PM2} = 1$, and $N_{RL,AR2} = 2$. As in [14], the system can be solved by factorizing $\mathcal{P}_{2D}$ and solving the resulting triangular systems [16], taking advantage of any symmetry, and the torques can be calculated using Maxwell's stress tensor, (19)-(21) in [14].

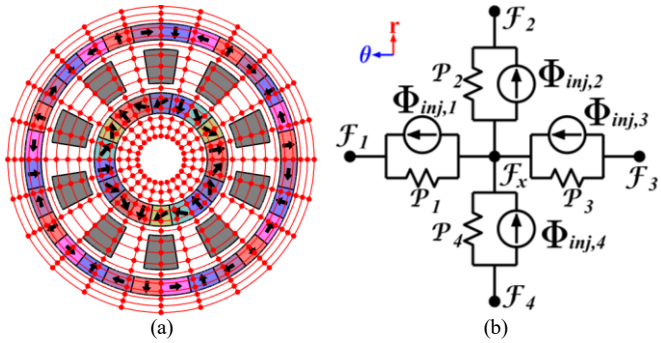

(a) (b)

Fig. 2. (a) Flux paths overlaid on an air core magnetic gear with Halbach arrays and (b) a 2D node cell with both radially and tangentially injected fluxes.

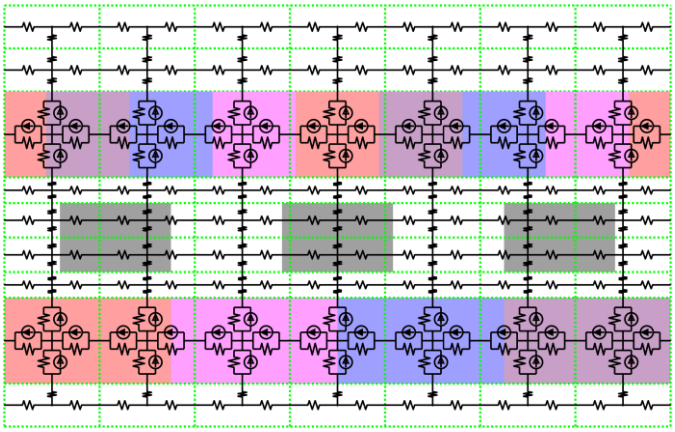

Fig. 3. Example 2D MEC schematic overlay on an unrolled radial flux air core magnetic gear geometry with Halbach arrays.

III. Base Designs

In order to investigate the performance of the MEC and the impact of the new discretization parameters, three base designs were selected for initial comparisons between the FEA and MEC results. The design parameters of these three base cases are listed in Table I, and their cross-sections are illustrated in Fig. 4. These base designs are not intended to be optimal; instead, they are selected to represent significantly different points in the design space. All designs evaluated in this study use NdFeB N42 PMs with a remanence of 1.3 T and M47 electrical steel for the modulators. In the MEC model, the modulators are assumed to have a relative permeability of 3000 and a 50% fill factor, as in [15]. Additionally, the PMs have a 100% fill factor, and, for each rotor, all of the PMs are the same size.

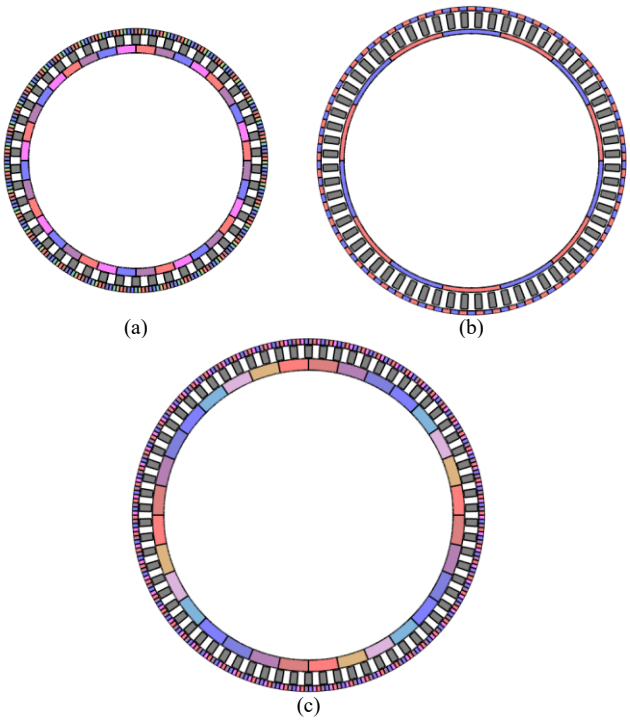

Fig. 4. Cross-sections of (a) Base Design 1, (b) Base Design 2, and (c) Base Design 3.

TABLE I. Base Designs for MEC Model Evaluation

Symbol	Description	Base Design 1	Base Design 2	Base Design 3
P_{In}	Inner pole pairs	9	7	4
P_{Out}	Outer pole pairs	37	57	66
N_{In}	PM segments per inner pole	2	1	4
N_{Out}	PM segments per outer pole	3	1	2
R_{Out}	Gear active outer radius (mm)	150	175	200
T_{PM1}	Inner PM radial thickness (mm)	9	5	13
T_{AG1}	Inner air gap thickness (mm)	0.5	2	1
T_{Mods}	Modulator radial thickness (mm)	11	17	14
T_{AG2}	Outer air gap thickness (mm)	0.5	2	1
T_{PM2}	Outer PM radial thickness (mm)	7	5	7

Fig. 5 illustrates the impact on the MEC model's accuracy as each of the new discretization parameters is swept along a range. In each case, the new discretization parameters that are not being swept are kept constant at their maximum values shown in the other graphs, 100 mm for T_{AR1}, 200 mm for T_{AR2}, 200 for $N_{RL,AR1}$, and 200 for $N_{RL,AR2}$. The other discretization parameters are maintained at the fine mesh values in Table III of [15]. As the value of each new discretization parameter is increased, the MEC model's stall torque for the modulator assembly (mods) converges to 102.4%, 99.7%, and 101.7% of that predicted by the FEA model for the three base designs, respectively. For convergence, Base Design 2 requires the largest value for most of the parameters because it has $N_{In} = 1$ and $N_{Out} = 1$, which results in significant flux leaking into the inner and outer air regions. However, Base Design 3 requires the largest outer air region thickness because it has the lowest pole count on the inner rotor, which results in longer flux paths from the inner rotor which extend further beyond the outer rotor.

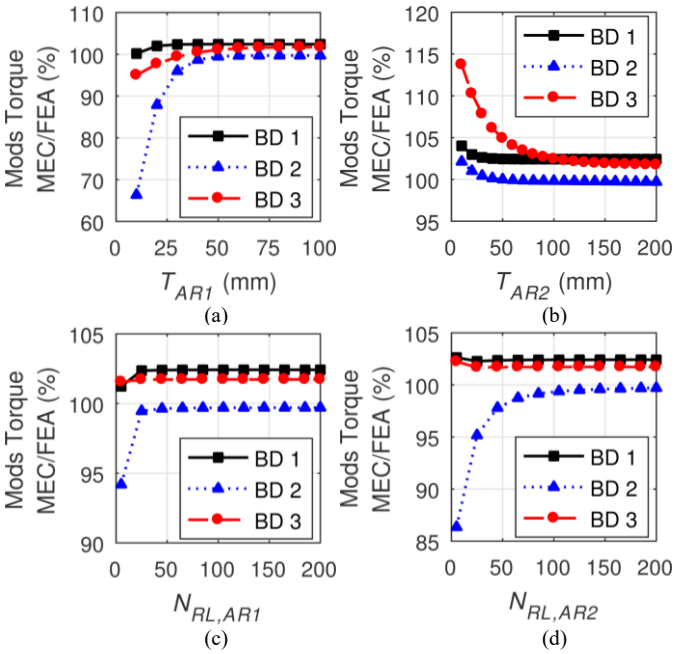

Fig. 5. Impact of (a) inner and (b) outer air region thicknesses included in the model and the number of radial layers in the (c) inner and (d) outer air regions on the accuracy of the MEC model relative to FEA simulations for each base design (BD).

Figs. 6 and 7 show the radial flux densities in the inner and outer air gaps at the stall torque point for each of the three base designs based on both the MEC and FEA models. The MEC models used for Figs. 6 and 7 have the same discretization parameter values as those on the rightmost edge of each of Figs. 5(a)-(d). For the most part, there is very good agreement between the two models. However, because the MEC model assumes the modulators are made from a material with fixed permeability, there is a small error for some of the flux density peaks. This linearity error causes the most discrepancies for Base Design 1, which is why it converges to the highest error.

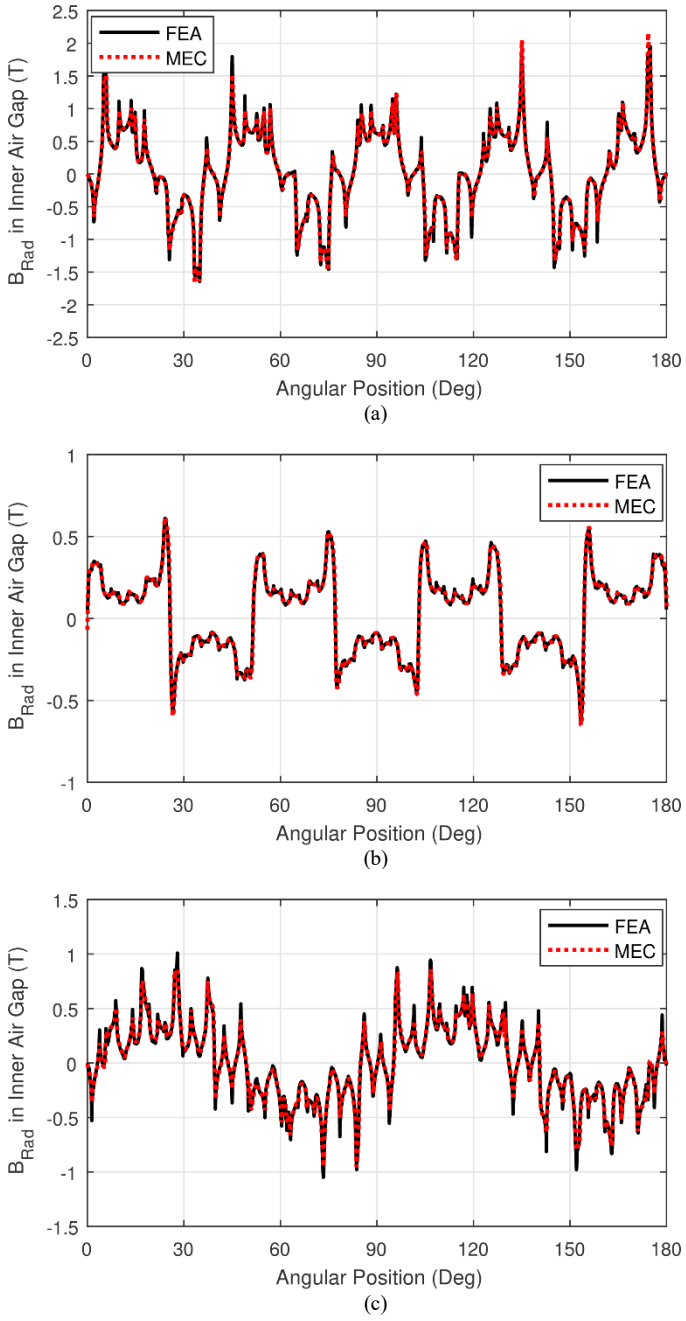

Fig. 6. Comparison of MEC and FEA radial flux densities in the inner air gaps of (a) Base Design 1, (b) Base Design 2, and (c) Base Design 3.

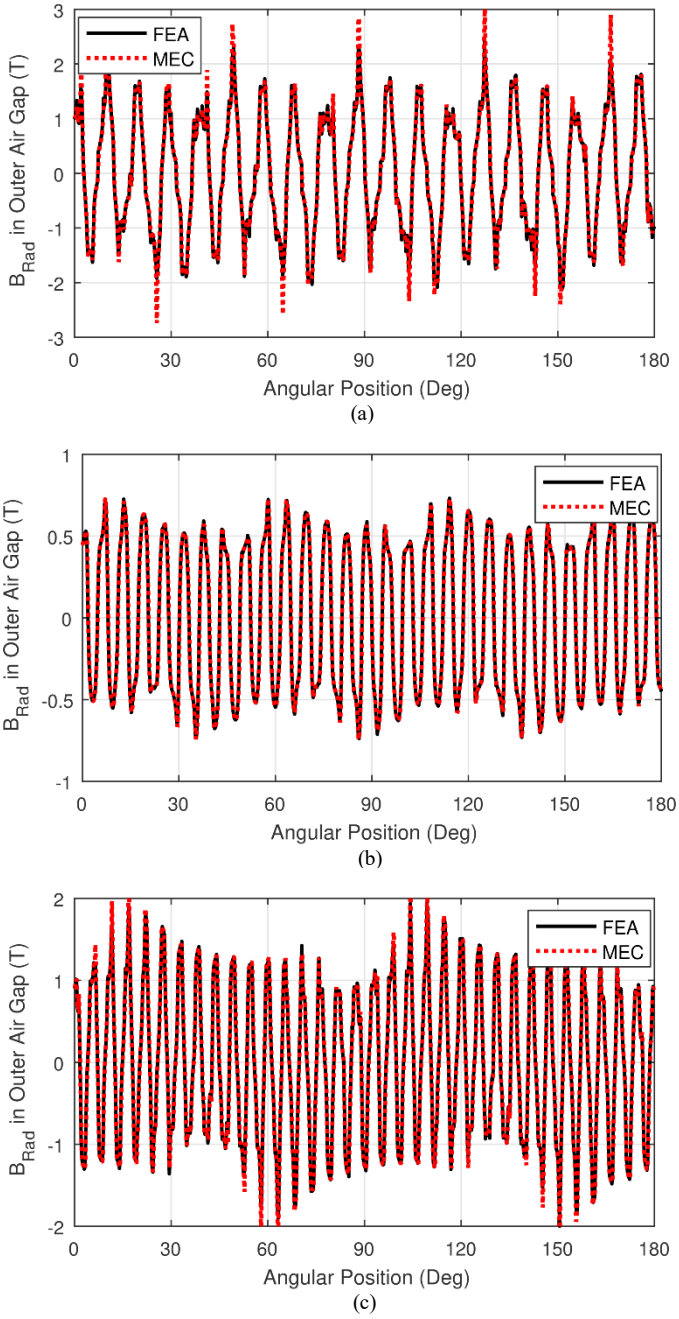

Fig. 7. Comparison of MEC and FEA radial flux densities in the outer air gaps of (a) Base Design 1, (b) Base Design 2, and (c) Base Design 3.

IV. Discretization Parameter Guidelines

It is necessary to develop guidelines for setting the values of the new MEC discretization parameters to achieve a consistent level of accuracy without using an excessive number of nodes, which would increase simulation times. Thus, the value of each of the four new parameters is tied to the pole arcs of the gear. First, T_{AR1} is determined by the inner pole arc based on the inner air region thickness multiplier, m_{AR1}, according to

$$T_{AR1} = \frac{\pi \, m_{AR1} \, R_{In}}{P_{In}}. \tag{6}$$

T_{AR2} is also tied to the pole arc determined by the inner pole count with the outer air region thickness multiplier, m_{AR2}, according to

$$T_{AR2} = \frac{\pi\, m_{AR2}\, R_{Out}}{P_{In}}. \quad (7)$$

T_{AR2} is tied to the inner pole count, instead of the outer pole count, because the inner pole count is much lower than the outer pole count, which results in much longer flux paths. The outer air region must be large enough to capture these flux paths from the inner rotor, which extend beyond the outside of the gear.

$N_{RL,AR1}$ is related to the inner pole arc by the inner air region layer multiplier, k_{AR1}, according to

$$N_{RL,AR1} = \frac{k_{AR1}\, T_{AR1}\, P_{In}}{\pi\, R_{In}}. \quad (8)$$

Similarly, $N_{RL,AR2}$ is related to the outer pole arc by the outer air region layer multiplier, k_{AR2}, according to

$$N_{RL,AR2} = \frac{k_{AR2}\, T_{AR2}\, P_{Out}}{\pi\, R_{Out}}. \quad (9)$$

Fig. 8 illustrates the same information as Fig. 5 but in terms of the multipliers, instead of the air region thicknesses and layer counts. Relative to these multipliers, Base Designs 1 and 3 generally seem to converge at roughly similar rates. However, because Base Design 2 has a single PM segment per pole, it experiences more leakage flux and needs higher multipliers to converge, especially k_{AR2}.

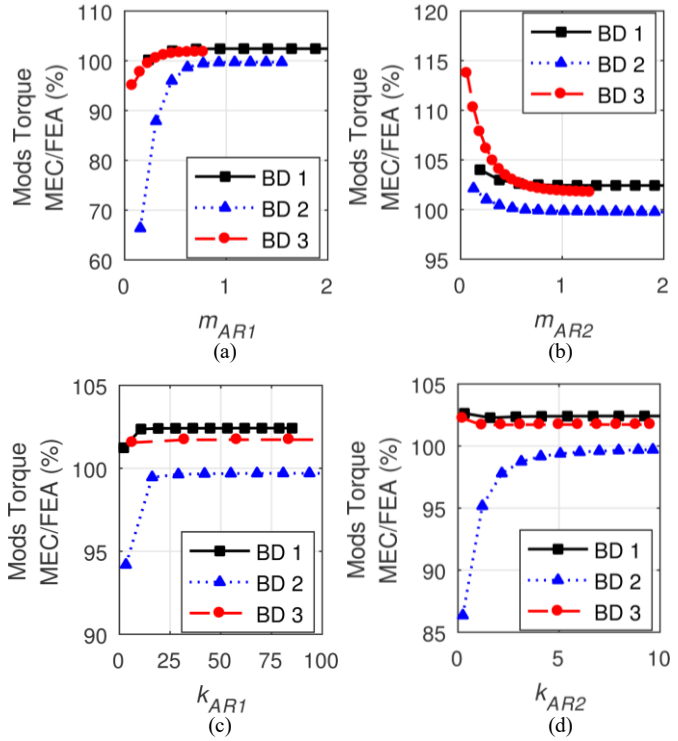

Fig. 8. Impact of (a) inner and (b) outer air region thickness multipliers and the (c) inner and (d) outer air region layer multipliers on the accuracy of the MEC model relative to FEA simulations for each base design (BD).

V. Optimization Study

For the MEC to be useful as an analysis tool, it must converge quickly to the optimal designs in a design study. Therefore, a wide range of designs was evaluated with both the MEC and the FEA to illustrate how accurate the MEC is across the design space and to determine whether it accurately captures design trends. A wide range of designs is also critical to ensure that the mesh settings consistently yield a high level of accuracy. A set of discretization settings may be accurate for a few designs because positive and negative errors cancel each other out. For example, the positive error from T_{AR2} being too small could be canceled out by the negative error from T_{AR1} being too small. However, such a situation is unlikely to yield consistently accurate results across a wide range of designs. Table II provides the values of the design parameters considered in this design study, using some derived parameters, as in [17], [18]. G_{Int} provides the integer part of the gear ratio (assuming the outer rotor is fixed) and relates the pole counts according to

$$P_{Out} = \begin{cases} (G_{Int}-1)P_{In}+1 & \text{for } G_{Int}\, P_{In} \text{ odd} \\ (G_{Int}-1)P_{In}+2 & \text{for } G_{Int}\, P_{In} \text{ even} \end{cases}. \quad (10)$$

This relationship keeps the modulator count even, which results in the cancellation of the magnetic forces on each rotor due to symmetry. Additionally, this relationship maintains a high least common multiple between the inner and outer pole pair counts, which results in designs with minimal torque ripple [5]. Furthermore, the PM thicknesses are related by k_{PM} according to

$$T_{PM2} = k_{PM}\, T_{PM1}. \quad (11)$$

This relationship is used to avoid designs where most of the PM material is placed on the outer rotor. Because the outer rotor has a much higher pole count than the inner rotor, there is much more flux leakage between adjacent poles on the outer rotor than on the inner rotor, so it is best to avoid designs with the outer PMs thicker than the inner PMs. The primary metric used to evaluate a design's performance in this study is its gravimetric torque density (GTD), which is defined as the stall torque of the modulator assembly divided by the total mass of the PMs and modulators in the design.

TABLE II. Optimization Study Design Parameters

Symbol	Description	Values	Units
G_{Int}	Integer part of gear ratio	5,9,17	
P_{In}	Inner pole pairs		
	For $G_{Int}=5$	4,7,10,…,19	
	For $G_{Int}=9$	3,5,7,…,13	
	For $G_{Int}=17$	3,4,5,…,8	
N_{In}	PM segments per inner pole	1,2,3,4	
N_{Out}	PM segments per outer pole	1,2,3	
R_{Out}	Gear active outer radius	150,175,200	mm
T_{PM1}	Inner PM radial thickness	3,7,11	mm
T_{AG1}	Inner air gap thickness	1.5	mm
T_{Mods}	Modulator radial thickness	11,14,17	mm
T_{AG2}	Outer air gap thickness	1.5	mm
k_{PM}	PM thickness ratio	0.5,0.75,1	

TABLE III. NEW DISCRETIZATION SETTINGS

Symbol	Description	Coarse Mesh	Fine Mesh
m_{AR1}	Inner air region thickness multiplier	0.57	0.8
m_{AR2}	Outer air region thickness multiplier	0.33	0.5
k_{AR1}	Inner air region layer thickness multiplier	7.5	10
k_{AR2}	Outer air region layer thickness multiplier		
	For $N_{In} = 1$	15	20
	For $N_{In} > 1$	7.5	10
$T_{AR1,min}$	Minimum inner air region thickness	5 mm	5 mm
$T_{AR1,max}$	Maximum inner air region thickness	R_{In}–5 mm	R_{In}–5 mm
$T_{AR2,min}$	Minimum outer air region thickness	5 mm	5 mm
$N_{RL,AR1,min}$	Minimum inner air region radial layers	3	3
$N_{RL,AR2,min}$	Minimum outer air region radial layers	3	3

Based on the results for a wide range of designs, two sets of values were chosen for the new multipliers, as shown in Table III. The fine mesh multipliers are used together with the fine mesh settings from Table III in [15], and the coarse mesh multipliers are used together with the coarse mesh settings from Table III in [15]. Note that in cases where (8) or (9) would yield a non-integer, the number of layers was rounded up. Additionally, an upper bound was placed on T_{AR1}, based upon the inner radius of the gear, R_{In}, to maintain a positive inner radius for the inner air region included in the MEC.

Figs. 9-12 illustrate the trends for the maximum achievable GTD's as each of the design parameters is varied. These figures illustrate that the GTD trends predicted by the MEC are in very good agreement with those predicted by the FEA. Thus, any optimization using the MEC will converge to a similar design as an optimization using FEA. This also indicates that the discretization settings in Table III do not bias the results of the MEC for any of the swept parameters, at least within the ranges considered in Table II. As in [15], the linear MEC will become inaccurate in designs where the modulator saturation becomes significant, such as designs with modulators have very small radial thicknesses or very low fill factors.

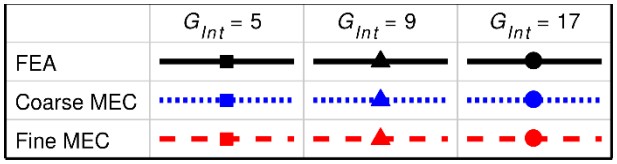

Fig. 9. Legend for Figs. 10-12.

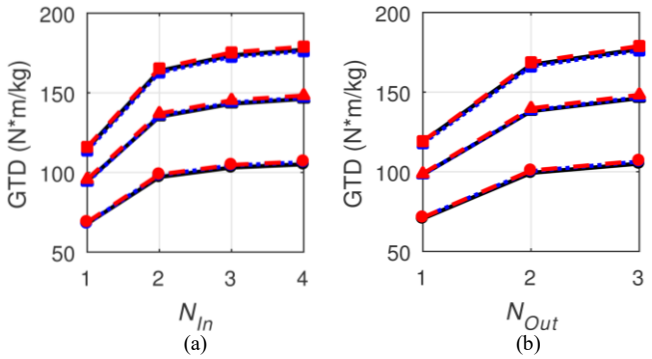

Fig. 10. Variation of the maximum achievable gravimetric torque density with the numbers of (a) inner and (b) outer of PM segments per pole.

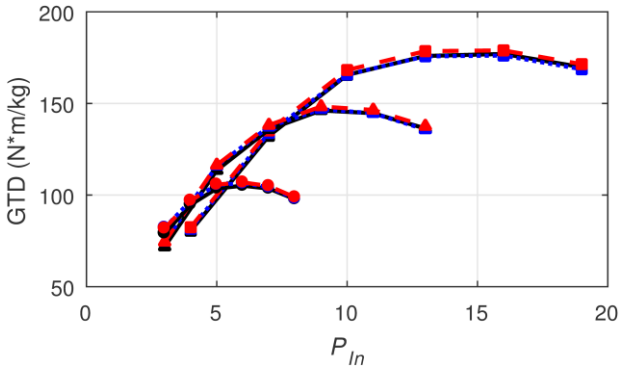

Fig. 11. Variation of the maximum achievable gravimetric torque density with the number of inner pole pairs.

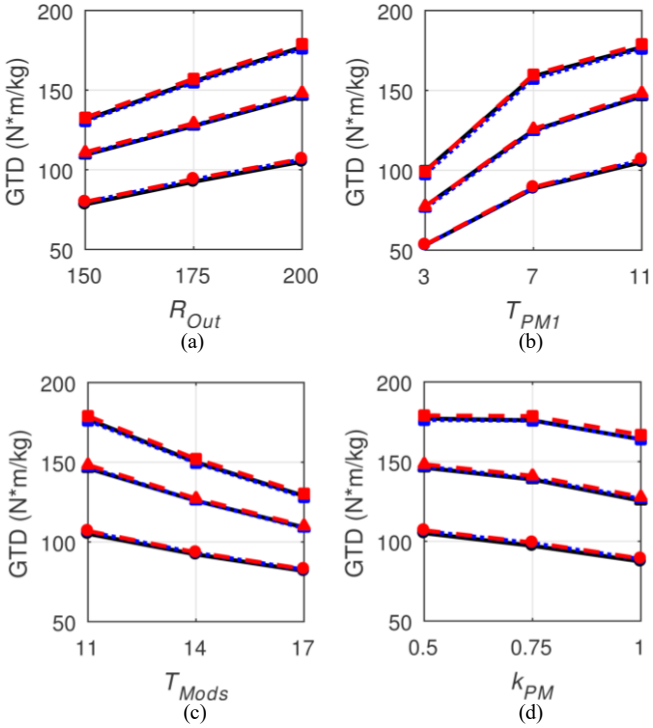

Fig. 12. Variation of the maximum achievable gravimetric torque density with (a) the outer radius, (b) the inner PM thickness, (c) the modulator thickness, and (d) the PM thickness ratio.

The performance of the MEC relative to the nonlinear FEA is illustrated in Fig. 13 and Table IV across the range of cases evaluated in the design study. While the MEC generally produces relatively low errors for the optimal designs, some of the less optimal designs do result in larger discrepancies between the torques predicted by the MEC and the FEA. The coarse mesh results in larger errors than the fine mesh; however, the coarse mesh produces much smaller permeance matrices, which can be evaluated significantly faster than the permeance matrices resulting from the fine mesh. With either mesh, the MEC is significantly faster than the FEA. (All MEC and FEA evaluations were performed on the same computer to avoid biasing the simulation times reported in Table IV. Additionally, the FEA used the same settings as in [15].) For both the MEC and the FEA, the cases with lower pole counts generally take much less time to evaluate than cases with higher pole counts.

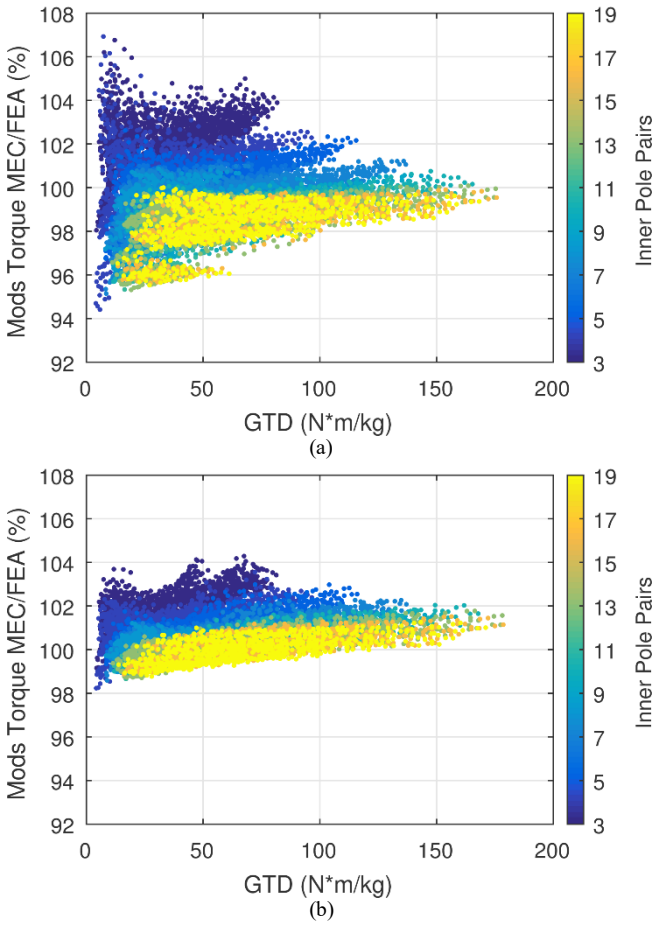

Fig. 13. MEC accuracy over the full parametric optimization sweep range using (a) the coarse mesh and (b) the fine mesh.

TABLE IV. SUMMARY OF OPTIMIZATION STUDY RESULTS

Metric	Coarse Mesh MEC	Fine Mesh MEC	FEA
Minimum Percent Error	-5.6%	-1.8%	N/A
Maximum Percent Error	6.9%	4.2%	N/A
Average Percent Error	-0.4%	0.6%	N/A
Average Absolute Percent Error	1.3%	0.8%	N/A
Total Simulation Time (sec)	7,160	112,000	659,000
Average Simulation Time (sec)	0.41	6.4	38

VI. CONCLUSION

A systematic linear 2D MEC implementation is proposed for coaxial radial flux magnetic gears with Halbach arrays and no back irons. Three base designs are evaluated to verify the accuracy of the MEC. With enough node cells, the torque predicted by the MEC converges to within 2.4%, 0.3%, and 1.7% of the torque predicted by a nonlinear 2D FEA for the three cases. Additionally, the air gap flux densities predicted by the MEC and the FEA show very good agreement for each of the three cases.

To further validate the usefulness of the MEC, an extensive parametric study is performed with both the MEC and the FEA. Guidelines are used to determine the node cell distribution based on the pole arcs of each design. With a relatively coarse mesh, the torques predicted by the MEC are in the range of 94-107% of those predicted by the FEA, with the predicted torques being within 1.3% of the FEA predictions on average. With a finer mesh, the torque range was limited to 98-104% of the FEA predictions, with the predicted torques being within 0.8% of the FEA predictions on average. The coarse mesh MEC was almost two orders of magnitude faster than the FEA, and the fine mesh MEC was about a factor of 5 times faster than the FEA. For both mesh conditions, the MEC accurately predicted the impact of each design parameters on torque performance. The MEC also accurately tracked the design trends associated with each parameter swept in the parametric study. Thus, the MEC can be used as an effective tool for rapid initial evaluation of a large number of designs.

This systematic MEC approach can be extended in a few ways. First, the node cell network can be extended to the third dimension to evaluate the impact of end-effects. Additionally, this MEC approach can be applied to conventional electric machines or to other topologies of magnetic gears. However, iron saturation introduces much more nonlinearity in conventional electric machines, so the MEC permeance matrix will need to be nonlinear and likely require an iterative solution.

ACKNOWLEDGMENTS

The authors would like to thank ANSYS for their support of the EMPE lab through the provision of FEA software.

REFERENCES

[1] K. Atallah and D. Howe, "A novel high-performance magnetic gear," *IEEE Trans. Magn.*, vol. 37, no. 4, pp. 2844–2846, Jul. 2001.

[2] P. O. Rasmussen, T. O. Anderson, F. T. Jorgensen, and O. Nielsen, "Development of a High Performance Magnetic Gear," *IEEE Trans. Ind. Appl.*, vol. 41, no. 3, pp. 764-770, May/June 2005.

[3] K. K. Uppalapati, M. D. Calvin, J. D. Wright, J. Pitchard, W. B. Williams, and J. Z. Bird, "A Magnetic Gearbox with an Active Region Torque Density of 239 N·m/L," *IEEE Trans. Ind. Appl.*, vol. 54, no. 2, pp. 1331-1338, Mar./Apr. 2018.

[4] P. M. Tlali, R.-J. Wang, and S. Gerber, "Magnetic gear technologies: A review," in *Proc. Int. Conf. Elect. Mach.*, 2014, pp. 544–550.

[5] N. W. Frank and H. A. Toliyat, "Gearing ratios of a magnetic gear for wind turbines," in *Proc. IEEE Int. Elect. Mach. Drives Conf.*, 2009, pp. 1224–1230.

[6] L. N. Jian, K. T. Chau, D. Zhang, J. Z. Jiang and Z. Wang, "A Magnetic-Geared Outer-Rotor Permanent-Magnet Brushless Machine for Wind Power Generation," in *Proc. IEEE Ind. Appl. Annual Meeting*, 2007, pp. 573-580.

[7] M. Johnson, M. C. Gardner, H. A. Toliyat , S. Englebretson, W. Ouyang and C. Tschida, "Design, Construction, and Analysis of a Large Scale Inner Stator Radial Flux Magnetically Geared Generator for Wave Energy Conversion," in *Proc. IEEE Energy Convers. Congr. and Expo.*, 2017, pp. 5017-5024.

[8] K. K. Uppalapati, J. Z. Bird, D. Jia, J. Garner, and A. Zhou, "Performance of a magnetic gear using ferrite magnets for low speed ocean power generation," in *Proc. IEEE Energy Convers. Congr. and Expo.*, 2012, pp. 3348–3355.

[9] E. K. Hussain, K. Atallah, M. Odavic, R. S. Dragan and R. E. Clark, "Pseudo Direct Drive electrical machines for flight control surface actuation," in *Proc. IET Int. Conf. Power Elect. Mach. Drives*, 2016, pp. 1-6.

[10] C. Liu, J. Yu and C. H. T. Lee, "A New Electric Magnetic-Geared Machine for Electric Unmanned Aerial Vehicles," *IEEE Trans. Magn.*, vol. 53, no. 11, pp. 1-6, Nov. 2017.

[11] L. Jian and K. T. Chau, “A Coaxial Magnetic Gear With Halbach Permanent-Magnet Arrays,” *IEEE Trans. Energy Convers.*, vol. 25, no. 2, pp. 319-328, June 2010.

[12] L. Jian, K. T. Chau, Y. Gong, J. Z. Jiang, C. Yu and W. Li, “Comparison of Coaxial Magnetic Gears With Different Topologies,” *IEEE Trans. Magn.*, vol. 45, no. 10, pp. 4526-4529, Oct. 2009.

[13] M. Johnson, M. C. Gardner, and H. A. Toliyat, “Analysis of axial filed magnetic gears with Halbach arrays,” in *Proc. IEEE Int. Elect. Mach. Drives Conf.*, 2015, pp. 108-114.

[14] M. Johnson, M. C. Gardner and H. A. Toliyat, “A Parameterized Linear Magnetic Equivalent Circuit for Analysis and Design of Radial Flux Magnetic Gears—Part I: Implementation,” *IEEE Trans. Energy Convers.*, vol. 33, no. 2, pp. 784-791, June 2018.

[15] M. Johnson, M. C. Gardner and H. A. Toliyat, “A Parameterized Linear Magnetic Equivalent Circuit for Analysis and Design of Radial Flux Magnetic Gears—Part II: Evaluation,” *IEEE Trans. Energy Convers.*, vol. 33, no. 2, pp. 792-800, June 2018.

[16] T. A. Davis, “Algorithm 930: FACTORIZE: An Object-Oriented Linear System Solver for MATLAB,” *ACM Trans. Math. Softw.,* vol. 39, no. 4, pp. 1-18, Jul. 2013.

[17] M. Johnson, M. C. Gardner, and H. A. Toliyat, “Design Comparison of NdFeB and Ferrite Radial Flux Surface Permanent Magnet Coaxial Magnetic Gears,” *IEEE Trans. Ind. Appl.*, vol. 54, no. 2, pp. 1254-1263, Mar./Apr. 2018.

[18] M. C. Gardner, B. E. Jack, M. Johnson, and H. A. Toliyat, "Comparison of Surface Mounted Permanent Magnet Coaxial Radial Flux Magnetic Gears Independently Optimized for Volume, Cost, and Mass," *IEEE Trans. Ind. Appl.*, vol. 54, no. 3, pp. 2237-2245, May/June 2018.